ARTICLE OPEN

Ultrastretchable and wearable conductive multifilament enabled by buckled polypyrrole structure in parallel

Yimeng Li[1,2], Yaya Gao[1,2], Lizhen Lan[1,2], Qian Zhang[1,2], Leqian Wei[1,2], Mengqi Shan[1,2], Lamei Guo[1], Fujun Wang[1,2], Jifu Mao [1,2✉], Ze Zhang[3] and Lu Wang[1,2]

Stretchable conductive fibers have attracted much attention due to their potential use in wearable electronics. However, the ultra-high strain insensitive conductivity is hindered by mechanical mismatch in Young's modulus and failure of stretchable structures under large deformation. This challenge is addressed with a conductive and elastic multifilament made of the polyurethane monofilaments that are surface-coated with buckled polypyrrole (PPy) of which flexibility is improved by sodium sulfosalicylate. Such parallel conductive monofilaments with PPy buckling on surface reduce the influence of cracks in the conductive coating on the overall conductivity, displaying an ultra-high strain insensitive behavior (quality factor $Q = 10.9$). Remarkably, various complex forms of wearable electronic textiles made by this conductive multifilament maintain the strain-insensitive behavior of the original multifilament, even upon the large deformation of human joint. This multifilament with wrinkled PPy has attractive advantages in the application of super-stretched wearable electronic devices.

INTRODUCTION

In recent years, wearable electronic textiles such as sensors[1,2], energy harvesting and storage devices[3,4], memory devices[5], displays[6] and heaters[7] have attracted an increasing interest from both research and industrial communities. The high-speed growth of wearable electronic textiles places a high demand on flexible and stretchable electronic circuit to ensure the stable and lossless transmission of electrical signals under a large mechanical stretch[8,9]. Various technological methods including helical coil structure[10,11], "twining spring" structure[12], layered structure[13], and buckled structure[8,14] have been developed to fabricate the stretchable electronic circuit toward designing multifunctional fibers and yarns. The most commonly used strategy relies on the geometrical constructions based on coiled spring principles, enabling stretchable electronics of high performance[10,11]. Despite the effectiveness of the method, disadvantages such as the multidimensional structures that often require complex bonding materials and bonding technology, and the non-planar movement of the coils during stretching, instigated the search for other alternative strategies[15]. The conductive fibrous composites with a spirally layered structure formed by rolling the films only provide an unsatisfactory solution for their low strain-insensitive behavior (quality factor $Q = 0.57$ at 356%)[13]. Therefore, a fiber-based stretchable electronic circuit with easy integration and high strain-insensitive behavior is still extremely desirable for wearable electronic textiles.

Buckling structures have been used to overcome spatial constraints while maintaining a constant conductivity in various flexible devices[16]. The apparent modulus of the conducting elements can be significantly lowered by forming the buckled structures, e.g., curled, wavy and wrinkled, on surface of the elastic substrate, guaranteeing the stretchability of the conductive fiber-based circuit[17]. For example, a worm-shaped conductive multi-filament was prepared by firstly pre-stretching a polyurethane

(PU) multifilament core and then coating it with a layer of graphene[8]. Such a structure enabled a negligible resistant change (about 0.26) up to 300% deformation. However, an increase in electrical resistance was observed at the initial stage of stretching due to the separation of the graphene wrinkles, a useful property for sensors[18,19] but undesirable for stretchable electronic circuits. Furthermore, although the buckled structure has been proved being able to effectively alleviate the mechanical mismatching between the conducting elements and substrate, a high interfacial interaction is always required to enhance the cycle performance[17]. Thus, it is critical to select the conducting elements for different substrates in order to obtain a superior interfacial interaction.

The conductive elements used in stretchable electronics mainly include metal nanowires[20], carbon nanomaterials[8], and conductive polymers[21,22]. Some of the most commonly used coating methods for the first two include spraying and dip-coating. The damage and debonding at the interface during stretching were reported, showing the necessity to further increase the interfacial interactions between the conductive elements and the substrate[17,23]. In contrast, a strong interfacial interaction between conductive polymers and substrates can be achieved by a simple in-situ polymerization method. On the other hand, conducting polymers are more compatible with elastomeric substrates in mechanical properties than with metal nanowires and carbon nanomaterials[17]. Among conductive polymers, polypyrrole (PPy) has attracted a great attention because of its lightweight, low cost, good electrical conductivity, and good biocompatibility[24]. However, the mechanical mismatch in Young's modulus, fracture tensile strain and tensile strength between PPy and an elastomeric substrate still exists even though they are all polymers. Consequently, a flexible (i.e., low Young's modulus) PPy coating is essential to achieve a superior stretchability.

Herein, inspired by the structure of the electrically sensitive muscle fiber bundles, we designed a conductive and elastic fiber

[1]Key Laboratory of Textile Science & Technology of Ministry of Education and College of Textiles, Donghua University, Shanghai 201620, China. [2]Key Laboratory of Textile Industry for Biomedical Textile Materials and Technology, Donghua University, Shanghai 201620, China. [3]Département de chirurgie, Faculté de médecine, Université Laval; Axe médecine régénératrice, Centre de recherche du CHU de Québec - Université Laval, Québec (QC) G1V 0A6, Canada. ✉email: jifu.mao@dhu.edu.cn
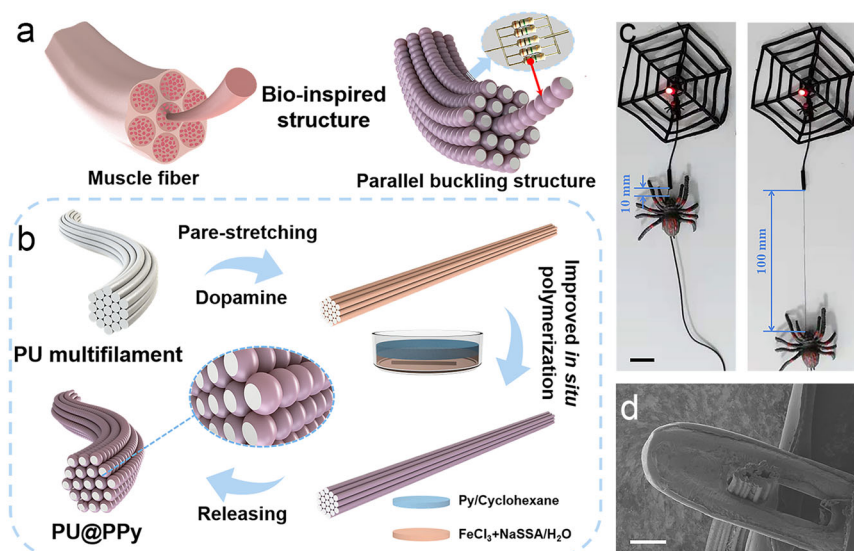
Fig. 1 The parallel PU monofilament with PPy buckling on surface, showing an ultra-high strain insensitive conductivity. a Prototypical model of the PU@PPy multifilament. **b** Schematic illustration of preparation of the conductive PU@PPy multifilament. **c** Optical images showing LED response to different elongations of the $PU_{200\%}^{420D}$ @PPy multifilament. Scale bar is 20 mm. **d** SEM image showing the $PU_{200\%}^{420D}$ @PPy multifilament passing through a #1 needle. Scale bar is 300 μm.

bundle made of the PU monofilaments that were surface-coated with buckled PPy *via* a simple in-situ polymerization method. Such parallel conductive monofilaments with PPy buckling on surface reduced the influence of cracks in the conductive coating on the overall conductivity, displaying an outstanding ultra-high strain insensitive behavior. Note that the flexibility of PPy was improved by adding sodium sulfosalicylate (NaSSA) as the plasticizer. This particular conductive multifilament exhibited a small diameter (0.21 mm), a good initial conductivity (238.0 S m^{-1}), and a remarkable strain-insensitive performance ($Q = 10.9$). Even at 900% tensile strain, it still maintained a stable electrical conductivity (relative resistivity change was only 3.5) and a recovery ability. More importantly, this conductive fiber can be easily integrated into the fabric by weaving, knitting, or embroidery. This integrable, highly stretchable, ultra-fine, and highly conductive PU multifilament is highly competitive for smart wearable textiles.

RESULTS AND DISCUSSION

Materials Design and Fabrication

Muscle tissue, the main contributor to a physiological movement, possesses an aligned structure composed of multiple fibers, and it is sensitive to electrical signals (Fig. 1a). Inspired by this structure, we developed the conductive multifilament based on two principles, i.e., strain insensitive conductivity under ultra-high strain and easy integration to wearable devices. For the latter requirement, undoubtedly, finer fibers will offer indubitable possibilities to be integrated into the compact and sophisticated electronic textiles. Similar to muscle fiber bundles, the conductive PU multifilament was made of multiple parallel monofilaments with the PPy buckling on surface, with the detailed fabrication process illustrated in Fig. 1b. PU_y^x @PPy denotes that the PU multifilament was *x* denier (D, one denier has a linear density of one gram mass per 9000 m of fiber) and the PPy coating was prepared under the pre-stretching strain *y*. Prior to in situ deposition of PPy, polydopamine (PDA) was introduced onto the surface of the pre-stretched PU multifilament to improve wettability *via* a DA coating-enhanced solution polymerization. An improved in situ polymerization method was adopted to obtain a homogeneous PPy coating layer on each monofilament

of the pre-stretched PU multifilament[25]. After releasing the stretch, the PPy wrinkles were formed on the surface of each monofilament. It is such a structure that gives the multifilament a stable conductivity under high strain. Hence, the brightness of the LED barely changed between 0% and 900% strain (Fig. 1c). In addition, the $PU_{200\%}^{420D}$ @PPy multifilament can possess a high conductivity at a small size. Thanks to its fine diameter, the conductive multifilament can pass through a #1 sewing needle, suggesting that it can be fabricated to wearable electronic devices with the existing textile technologies (Fig. 1d).

The limited flexibility of PPy due to its rigid conjugated backbone is the biggest obstacle to its application in stretchable conductors[26]. There were cracks under a small strain on surface of the $PU_{50\%}^{210D}$ @PPy multifilament when only FeCl$_3$ was used as the dopant (Supplementary Fig. 1). In this work, in addition to decreasing the apparent modulus of the PPy layer by structural design, NaSSA was used as a plasticizer to improve the intrinsic flexibility as well. The PPy films with or without NaSSA were synthesized *via* interfacial polymerization (more details can be found in the Supporting Information) to determine whether the incorporation of NaSSA indeed improved the mechanical property. As shown in Supplementary Fig. 2a-c, the breaking elongation of the PPy films with Cl$^-$/SSA$^-$ as dopant (PPy$_{FeCl_3/NaSSA}$) was 8.58%, which was much higher than that (3.81%) of the PPy film with Cl$^-$ as dopant (PPy$_{FeCl_3}$). A larger bending angle (51.20°) of the PPy$_{FeCl_3}$ film was further demonstrated by the cantilever method, confirming that the flexibility of the PPy film was enhanced by NaSSA (Supplementary Fig. 2d). The PPy$_{FeCl_3}$ film exhibited incredible capacity under repeated bending at room temperature (Fig. 2a). More interestingly, this flexibility was retained in liquid nitrogen (Fig. 2b and Supplementary Video 1). We have previously reported the pristine PPy membranes that are as soft in liquid nitrogen as at room temperature and discussed this interesting phenomenon as well[26,27]. In this work, the intrinsic properties were also believed to be the cause of flexibility of both PPy films and PPy coatings. Furthermore, it is contradictory for conductive polymers to have both high conductivity and high flexibility[28]. Excitingly, NaSSA could improve not only the flexibility of PPy but also the conductivity. The conductivity of PU@PPy increased from 70.8 ± 4.6 S m^{-1} to 358.2 ± 27.9 S m^{-1} after NaSSA was employed as dopant.
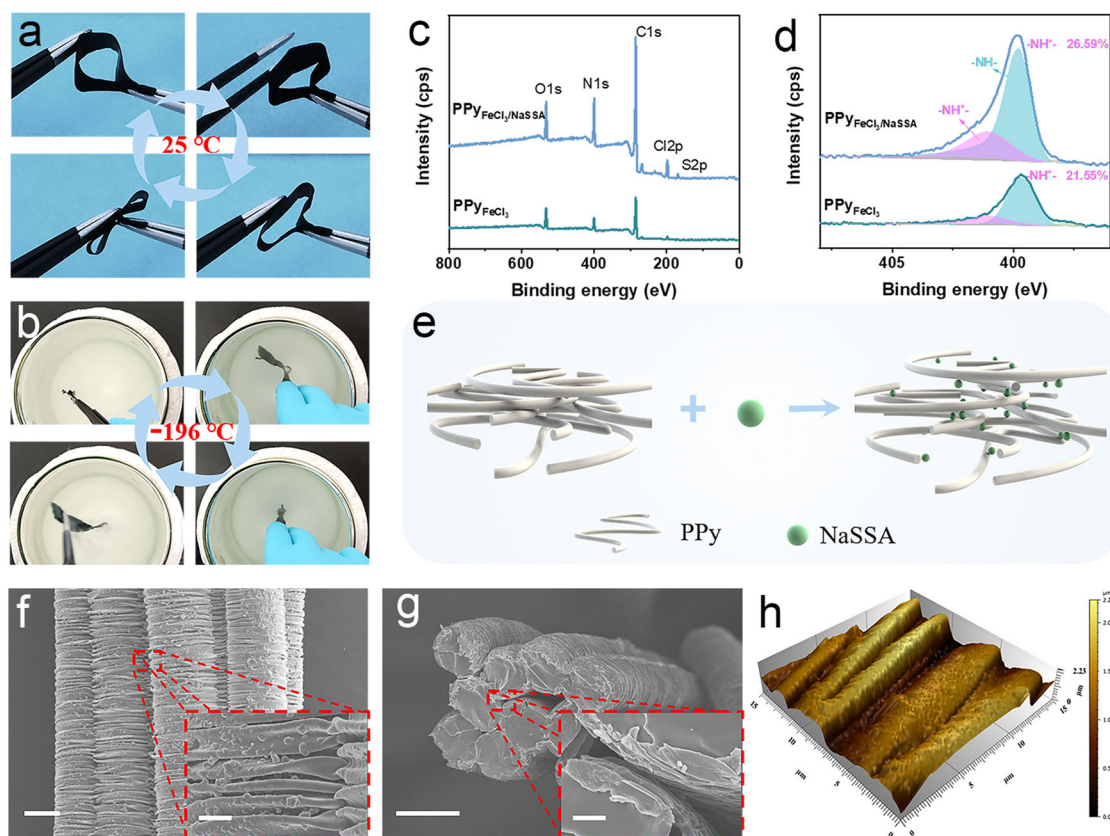
Fig. 2 **Characterization of the ultrastretchable PU@PPy multifilament. a** PPy films bending at room temperature. **b** PPy films waving in liquid nitrogen. **c** Full scan XPS spectra; High resolution spectra of **d** N1s of PPy films. **e** Schematic illustration of stretchable PPy with NaSSA as plasticizer. SEM images of the $PU_{300\%}^{210D}$ @PPy without PDA treatment from **f** longitudinal and **g** cross-section views. Scale bar is: 50 μm, inset 5 μm. **h** AFM image of the $PU_{300\%}^{210D}$ @PPy with PDA treatment.

To further explain the role of NaSSA in enhancing the conductivity and flexibility of PPy, the chemical analyses were explored using XPS and Raman spectrum. Sulfur (S) element was observed in the XPS spectrum of the PPy with FeCl₃/NaSSA as dopant, confirming that NaSSA acted as counter ions (Fig. 2c). And the relative content of $-NH^+-$ (26.59%) in the PPy with FeCl₃/NaSSA as dopant was higher than that (21.55%) in the specimen without doping of NaSSA, indicating that NaSSA could improve the conductivity of PPy by increasing the doping level (Fig. 2d). Raman spectra of the PU@PPy prepared with or without NaSSA as dopant was measured also. The spectrum (Supplementary Fig. 3) shows the main bands of PPy at 1576 cm⁻¹ (C = C stretching), 1374 and 1327 cm⁻¹ (two bands of ring-stretching), 1238 cm⁻¹ (antisymmetric C–H in plane bending), 1084 and 930 cm⁻¹ (the bipolaron structure), and 1046 and 963 cm⁻¹ (the polaron structure)[25]. The ratios between the bipolaron (1084 and 930 cm⁻¹) and polaron (1046 and 963 cm⁻¹) absorptions were used to estimate the degree of doping and these ratios are reported in Supplementary Table 1[29]. Higher bipolaron/polaron ratios of the PU@PPy prepared with NaSSA as dopant was considered as an evidence explaining that the NaSSA dopant enhanced the conductivity of PPy also. Sulfonate and sulfonimide anions have been reported to have a charge screening effect that weakens the interactions between polymers[28]. What is particularly important is that the doping of d-sorbitol could weaken the interactions between polymer chains to improve mechanical flexibility[30]. Therefore, we suspect that the NaSSA has two effects: 1. NaSSA molecules weakened the interactions between PPy chains (Fig. 2e), and so facilitated the movement of the molecular chains leading to a reduced intrinsic modulus of PPy; 2. NaSSA dopants increased the doping level of PPy, resulting in an improved conductivity.

To evaluate the effect of PDA on the buckling structure, the morphology of the $PU_{300\%}^{210D}$ @PPy multifilament with or without PDA treatment was observed (Fig. 2f–h and Supplementary Fig. 4a–c). PPy cracks along the fiber axis were only observed on the $PU_{300\%}^{210D}$ @PPy multifilament without PDA treatment (Fig. 2f and Supplementary Fig. 4a), indicating that the use of PDA prevented PPy from cracking. This was because that the PDA coating increased PPy deposition[31], resulting in a thick PPy coating that was more resistant to the circumferential expansion when the filament was released. Indeed, the thickness of the PPy on $PU_{300\%}^{210D}$ @PPy was 0.80 ± 0.17 μm, while that without PDA was only 0.54 ± 0.10 μm (Supplementary Fig. 4b and Fig. 2g). Further, the height of the bucklings on the PU@PPy with PDA modification (~1.56 μm) was much larger than that without PDA (~0.25 μm), as shown in Fig. 2h, Supplementary Fig. 5, and Supplementary Fig. 4c. Such differences in shape and size of the buckling structure were also caused by the thickness of the PPy coating (more detailed analysis can be found in Supplementary Method 1). Remarkably, the SEM images of the cross-sections revealed that each monofilament of the PDA modified multifilament was coated with buckled PPy, in contrast to the incomplete PPy coating on the unmodified monofilaments (Fig. 2g and Supplementary Fig. 4b). This is a fascinating structure that had rarely been observed and reported in literature so far.

To investigate the effect of polymerization time on the shape of the buckling, PPy was polymerized on the $PU_{300\%}^{210D}$ @PPy for different times. Compared to the smooth surface of the PU multifilament (Supplementary Fig. 6a), the surface of each parallel
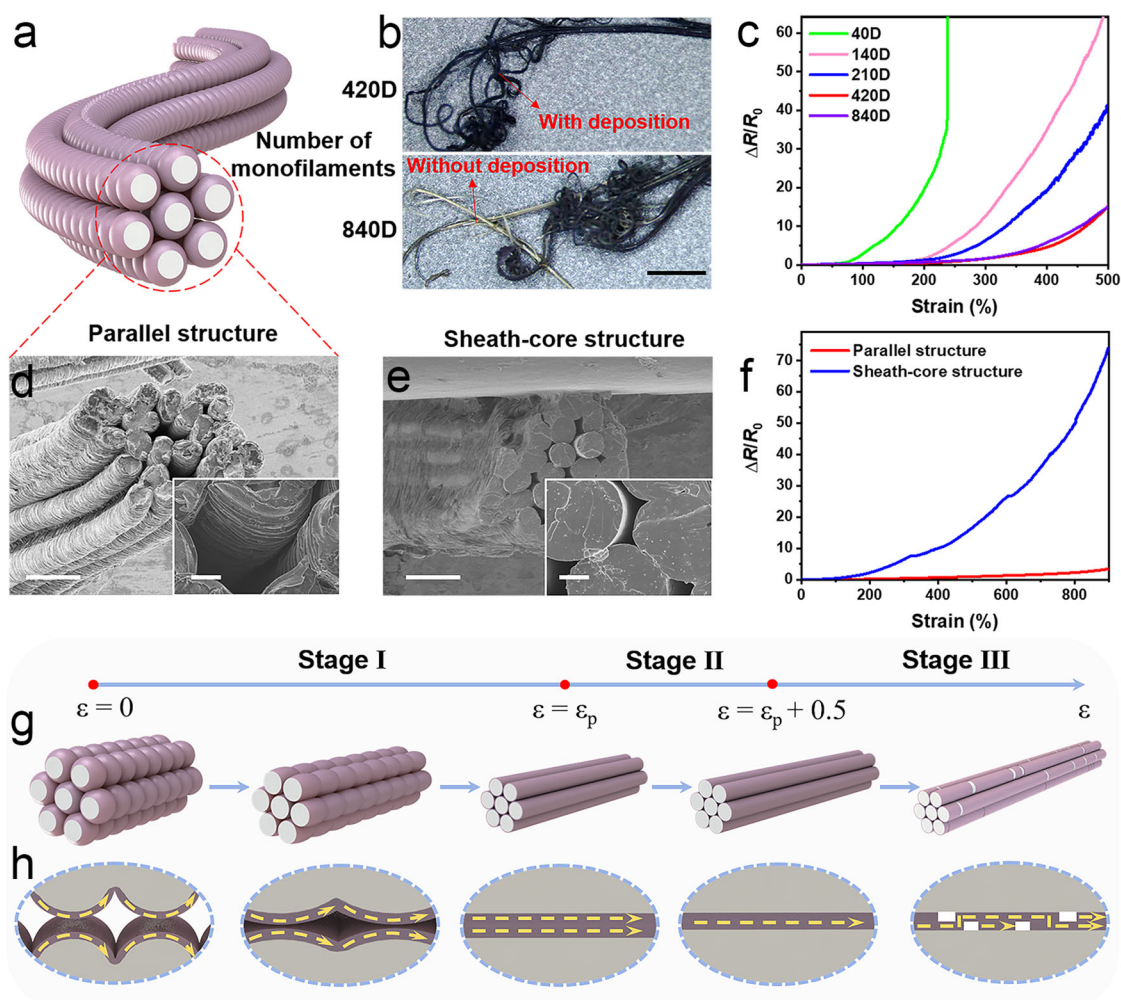
Fig. 3 Effect of the number of parallel conducting monofilaments on strain-insensitive behavior. a Schematic diagram of parallel conducting monofilaments with buckling PPy coating. **b** Optical photos of $PU_{50\%}^{420D}$ @PPy and $PU_{50\%}^{840D}$ @PPy after breaking. Scale bar is 2 mm. **c** Relative resistance change of $PU_{50\%}^{x}$ @PPy with different diameters upon increasing strain. SEM images of the cross-section of **d** $PU_{200\%}^{420D}$ @PPy and **e** $PU_{200\%}^{420D}$ @WPU@PPy. Scale bar is: 100 μm, inset 15 μm. **f** Change in relative resistance of the conductive multifilament and sheath-core filament under stretching. **g** Working mechanism of the parallel conductive multifilament under increasing strain. **h** Current path (yellow arrow) along the multifilament during stretching.

monofilament within the PU@PPy multifilament was fully covered by dense and regular wrinkles of PPy (Supplementary Fig. 6b-f). The presence of PPy was confirmed by the FTIR analysis according to the characteristic peak at 993 cm^{-1} assigned to the in plane stretching of =C-H (Supplementary Fig. 7)[32]. The highest conductivity (Supplementary Fig. 8) of and the densest bucklings (Supplementary Fig. 6) on the $PU_{300\%}^{210D}$ @PPy multifilament were obtained when the polymerization time was 24 h, which was considered as the optimal reaction time.

Mechanical properties

To elucidate the effects of the buckling structure on mechanical properties, we evaluated the PU@PPy multifilament made of a different number of monofilaments, the PU multifilament, and the PU_{y}^{420D} @PPy multifilament prepared under different pre-stretching strains (Supplementary Fig. 9). As the number of monofilaments increased, the breaking strength of the $PU_{50\%}^{x}$ @PPy multifilament gradually decreased, while the breaking elongation showed an opposite tendency (Supplementary Fig. 9a–c). The former was attributed to the increase in the probability of weak nodes as the number of monofilaments

increases, and the latter was related to the increase in the multifilament diameter[33]. The mechanical properties of PU without PPy coating also showed a similar trend, which makes us believe that this phenomenon was caused by the structure of the PU multifilament rather than the PPy coating (Supplementary Fig. 9d-f). The tensile properties of the PU_{y}^{420D} @PPy prepared under different pre-stretching strains were also evaluated (Supplementary Fig. 9g-i). Although the elongation of the multifilament gradually decreased with the increase of the pre-stretching strain, all the multifilaments exhibited an outstanding high stretchability (>1000%) and the similar strength at break (~100 MPa), in consistent with previous studies[8]. In addition, the $PU_{200\%}^{420D}$ @PPy multifilament showed a good recoverability within 100% strain, and a small hysteresis within 200% strain that is comparable to those in the reference (Supplementary Fig. 10a)[8,34]. After 100 loading-unloading cycles under 100% strain, the recovery performance of the multifilament was hardly deteriorated (Supplementary Fig. 10b). The strong strength and highly stretchable properties of the $PU_{200\%}^{420D}$ @PPy multifilament could guarantee the availability for the manufacture of large strain wearable electronic textiles.

Parallel structure and hypothetic model

The strain dependence of relative resistance change ($\Delta R/R_0$) of the $PU_{50\%}^{x}$ @PPy with different numbers of parallel monofilament was further evaluated to prove the function of parallel structure (Fig. 3a–c). As shown in Fig. 3c, all the $PU_{50\%}^{x}$ @PPy exhibited a similar strain-insensitive resistance change at low strain (< 50%) due to the analogous buckling-shaped PPy coating, of which the distance between the adjacent buckles was about 5 μm (Supplementary Fig. 11a-e). The buckled morphology is an important factor affecting the strain-insensitive behavior at low strain, as reported in previous studies[18,21]. When strain was further increased, the strain dependence of $\Delta R/R_0$ of the $PU_{50\%}^{x}$ @PPy decreased as the number of monofilaments increased. This was because even if the PPy coating on one monofilament broken, the PPy coatings on other monofilaments at the same cross-section might still be intact to allow electricity to flow through freely, thanks to the

disappearing free space among monofilaments during stretching to the ultra-high strains. Obviously, this probability increased as the number of monofilaments increased. The electro-response-to-strain of the $PU_{50\%}^{840D}$ @PPy was however not further reduced because the conductive coating failed to fully penetrate deep into the thick PU multifilament, i.e., 840D, confirmed by the white filaments rather than the black PPy coating inside the $PU_{50\%}^{840D}$ @PPy and exposed after its broken (Fig. 3b).

To more intuitively demonstrate the strain-insensitive performance of the conductive monofilament in parallel ($PU_{200\%}^{420D}$ @PPy, the SEM image of its cross-section is presented in Fig. 3d), and the sheath-core filaments with buckling-shaped PPy coating (Fig. 3e), named $PU_{200\%}^{420D}$ @WPU@PPy, were prepared as a control (See the Supporting Information for details). Figure 3f evidently illustrates that the $\Delta R/R_0$ of the $PU_{200\%}^{420D}$ @WPU@PPy multifilament was much
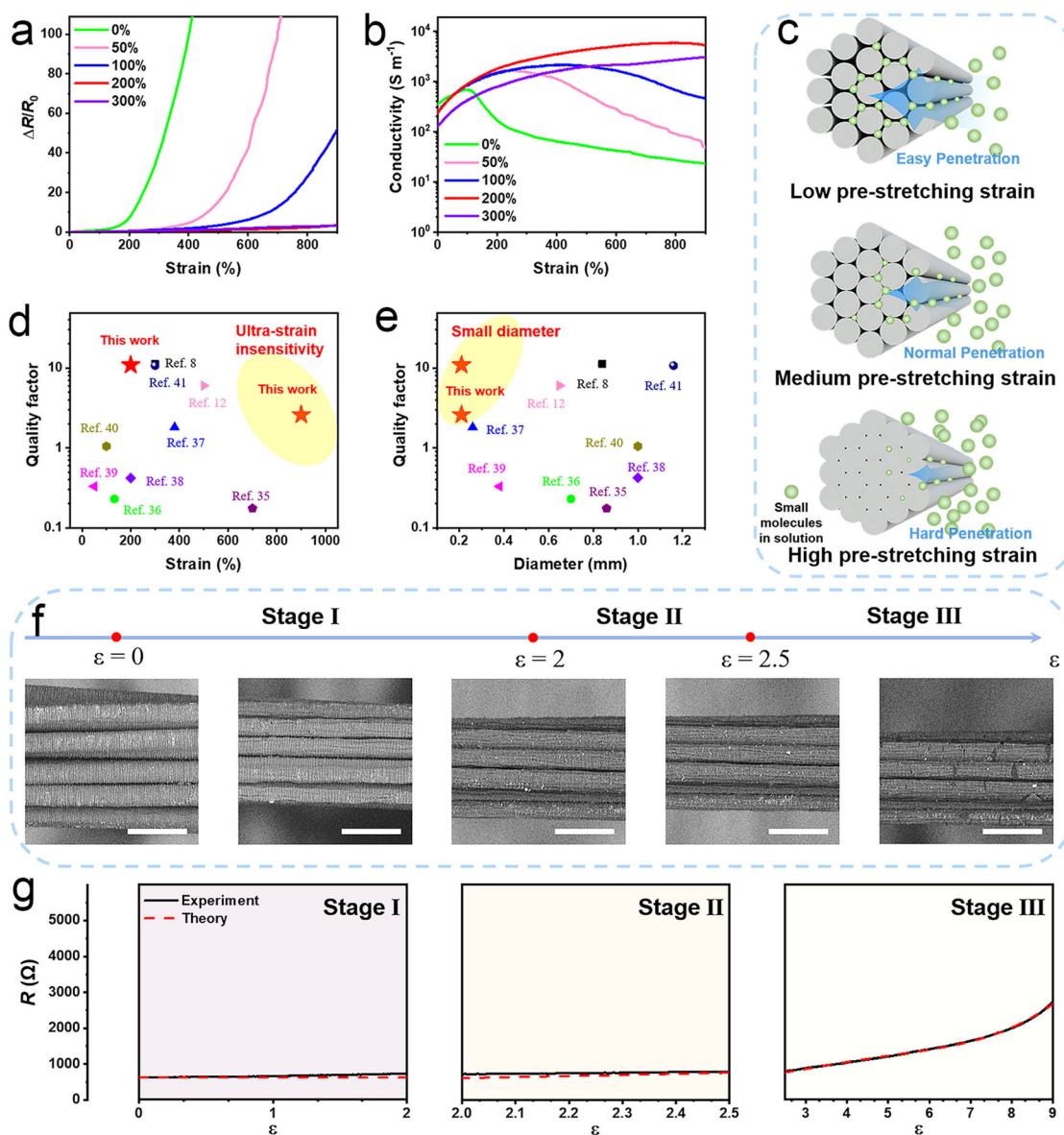

Fig. 4 Electrical properties of multifilament with different pre-stretching strains. a Relative resistance change of PU_{y}^{420D} @PPy upon increasing strain. **b** Conductivity-Strain curves of PU_{y}^{420D} @PPy. **c** The diagram of permeation effect of multifilament with different pre-stretching strains on small molecule (such as DA, FeCl$_3$, NaSSA, and Py represented by green spheres). **d-e** Comparison of $PU_{200\%}^{420D}$ @PPy with 1D conductor reported in the literature (Ref. [8,12,35–41]). **f** SEM images and **g** the resistance of $PU_{200\%}^{420D}$ @PPy under increasing strain. Scale bar is 100 μm.

higher than that of the $PU_{200\%}^{420D}$ @PPy under 200% strain (1.67 vs 0.18). More importantly, the $PU_{200\%}^{420D}$ @PPy exhibited better strain insensitive behavior, maintaining the $\Delta R/R_0$ at a low level (3.50) until the strain reached 900%, while that value of the $PU_{200\%}^{420D}$ @WPU@PPy increased sharply to 74.00.

In order to further explain the high strain insensibility of the PU@PPy conductor, a model was established to demonstrate how the PPy changed during stretching, as shown in Fig. 3g & h. The stretching process can be generally divided into three stages. In the first stage when the strain ε < pre-stretching strain ε_p, the PPy buckling gradually expands and the resistance remains constant resistance $R = R_0$, where R_0 is the initial resistance. Different from previous studies[8,35], our work didn't show the sharp increase in resistance caused by the reduction in contact area between adjacent buckles during stretching. An ordered buckling structure is showed by the AFM (Fig. 2h) and SEM images (Supplementary Fig. 11 & 12) of the PU@PPy multifilament. In the second stage where $\varepsilon > \varepsilon_p$, the PPy coating begins to show a tensile deformation, which is manifested by the decrease in the thickness and the increase in the length of the PPy coating. When Poisson effect is taken into consideration the resistance in this stage is given by Eq. (1).

$$R = \frac{(1+\varepsilon)(1+\varepsilon_p)}{(1+\varepsilon_p+\gamma\varepsilon_p-\gamma\varepsilon)^2}R_{\varepsilon_p} \quad (1)$$

where γ is the Poisson's ratio of PPy coating, and R_{ε_p} is the resistance of the PU@PPy at strain ε_p. More details can be found in Supplementary Method 2. Under excessive strain, cracks in PPy coating appear, hindering the flow of current. However, because the conductive monofilaments are independent each other, the cracks in one filament do not propagate to the surrounding monofilaments, and the tight junction among monofilaments under the high strain can guarantee the intact conductive path for electrical current. As shown in Supplementary Fig. 13, an equivalent resistance model is used to explain the electrical stability. The conductive multifilament can be regarded as numerous resistors in series along the longitudinal direction, and each resistor can be considered being composed by multiple parallel resistors along the perpendicular or cross-section direction (the number of the parallel resistors is the number of the conductive monofilaments). When cracks occur on some resistors, their conductivity drops dramatically; however, other resistors parallel with them still maintain conductivity. In this stage, the resistance can be calculated by Eq. (2).

$$R = \frac{2}{\frac{q\left(1+\varepsilon_p+\gamma\varepsilon_p-\gamma\varepsilon\right)^2}{(1+\varepsilon)(1+\varepsilon_p)}+p\left[1-erf\left(\ln\frac{\varepsilon-x}{(1+x)\varepsilon_0}/\mu\right)\right]} \quad (2)$$

where $erf(x)$ is the error function, and q, p, ε_0, and μ are fitting parameters. More details can be found in Supplementary Method 3.

Strain-insensitive conductivity and verification of model
Furthermore, the strain-insensitive properties of the conductive multifilament with different pre-stretching strains were studied (Fig. 4). As shown in Fig. 4a, the $\Delta R/R_0$ of all the PU_y^{420D} @PPy multifilament increased with the increase of tensile strain. And the rate of the increase in $\Delta R/R_0$ declined as the pre-stretching strain heightened, which was related to the buckling shape (Supplementary Fig. 12). The electrical conductivity of the stretchable PU_y^{420D} @PPy was further calculated with the volume of the multifilament assumed constant during stretching, as shown in Fig. 4b. With the increment in axial strain, conductivity of the $PU_{200\%}^{420D}$ @PPy multifilament increased from 238.0 S m^{-1} to 5304.0 S m^{-1}, which was consistent with the reported in literature[8,30]. This may be caused by the synergistic effect between the expansion of the PPy buckles and the stress-induced alignment of the conductive PPy chains[30]. Remarkably, the

$PU_{200\%}^{420D}$ @PPy exhibited a wide range of electro-response reversibility, no downward trend up to the ultra-high strain of 900%. Such a behavior was ascribed to the parallel structures that have the capacity to provide the additional conductive path under ultra-high strain due to the tight contact among monofilaments. The strain-insensitive performance of the $PU_{200\%}^{420D}$ @PPy and the $PU_{300\%}^{420D}$ @PPy was similar (Fig. 4a) because that the tiny free space among monofilaments under a high tensile strain made PPy difficult to penetrate into the PU multifilament (Fig. 4c), which was supported by the cross-section observation of the PU_y^{420D} @PPy (Supplementary Fig. 14) and by the weight percentage of PPy (Supplementary Fig. 15 and Supplementary Table 2). This trend was common to other PU@PPy of different numbers of parallel conductive monofilaments (Supplementary Fig. 16). Moreover, the initial conductivity of the PU_y^{420D} @PPy multifilament decreased from 344.1 S m^{-1} to 125.4 S m^{-1} when pre-stretching strain increased from 0% to 300% (Fig. 4b), which also indicates that the adjacent buckles are independent, i.e., not in contact (Supplementary Fig. 12) and the reduction of the weight percentage of PPy in the multifilament resulting from the difficulty for PPy to penetrate into the tight PU multifilament under the high pre-stretching strain (Supplementary Fig. 15 and Supplementary Table 2).

In addition, the electrical conductivity of the PU_y^{420D} @PPy with different pre-stretching strains was evaluated by the I-V curve under 5 V on-load voltage (Supplementary Fig. 17). All the multifilaments exhibited a linear shape, indicating that the multifilament obeys the Ohm's law. And the decrease in the slope of the curves also confirmed that the resistance of the PU_y^{420D} @PPy multifilament increased after the pre-stretching strain treatment.

The quality factor $Q = (\Delta l/l_0)/(\Delta R/R_0)$ was adopted to further evaluate the strain-insensitive behavior of the $PU_{200\%}^{420D}$ @PPy[14]. Compared with the 1D linear stretchable conductors reported in literature[8,12,35–41], the $PU_{200\%}^{420D}$ @PPy exhibited a much larger Q factor under ultra-strain and fineness (Fig. 4d & e, detailed data can be found in Supplementary Table 3). As shown in Fig. 4d, the Q factor of the $PU_{200\%}^{420D}$ @PPy was 10.9 at a 200% elongation, which is among the best compared with the literature. The Q then remained at 2.6 for up to 900%, demonstrating the good strain-insensitive behavior of this conductive multifilament under ultra-high strain. Remarkably, the diameter of the multifilament is only about 0.21 mm that is much smaller than any other reported conductors (Fig. 4e), offering great possibilities for its integration in smart wearable devices.

To test the above hypothetic model of the parallel conductive monofilament under increasing strain, in situ tensile test was performed using the SEM equipped with a Tensile Holder (Fig. 4f and Supplementary Videos 2–4). The PPy buckles on the $PU_{200\%}^{420D}$ @PPy surface gradually expanded as stretching (Supplementary Video 3), while the PPy coating on the $PU_{0\%}^{420D}$ @PPy surface started to crack at about 45% strain (Supplementary Video 2). To observe the three stages of change in PPy coating, a stretched $PU_{200\%}^{420D}$ @PPy (strain between 150% and 200%) was held on the stretching table of in situ SEM tensile. The Supplementary Video 4 recorded the above three stages in the stretching process of the $PU_{200\%}^{420D}$ @PPy, ratified our model and the assumptions. The γ in Eq. (2) for the $PU_{200\%}^{420D}$ @PPy was obtained from Supplementary Video 2. Equation (3) provides the resistance of the $PU_{200\%}^{420D}$ @PPy during the stretching process.

$$R = \begin{cases} R_0 & 0 \leq \varepsilon \leq 2 \\ \frac{3(1+\varepsilon)R_0}{(3.4-0.2\varepsilon)^2} & 2 < \varepsilon \leq 2.5 \\ \frac{2}{\frac{0.0007(3.4-0.2\varepsilon)^2}{1+\varepsilon}+0.0005(1-erf(2.19ln(\varepsilon-2.5)-4.255))} & 2.5 < \varepsilon \leq 9 \end{cases} \quad (3)$$

The theoretical resistance of the $PU_{200\%}^{420D}$ @PPy during stretching is shown in Fig. 4g, which well fitted the experiment data. The
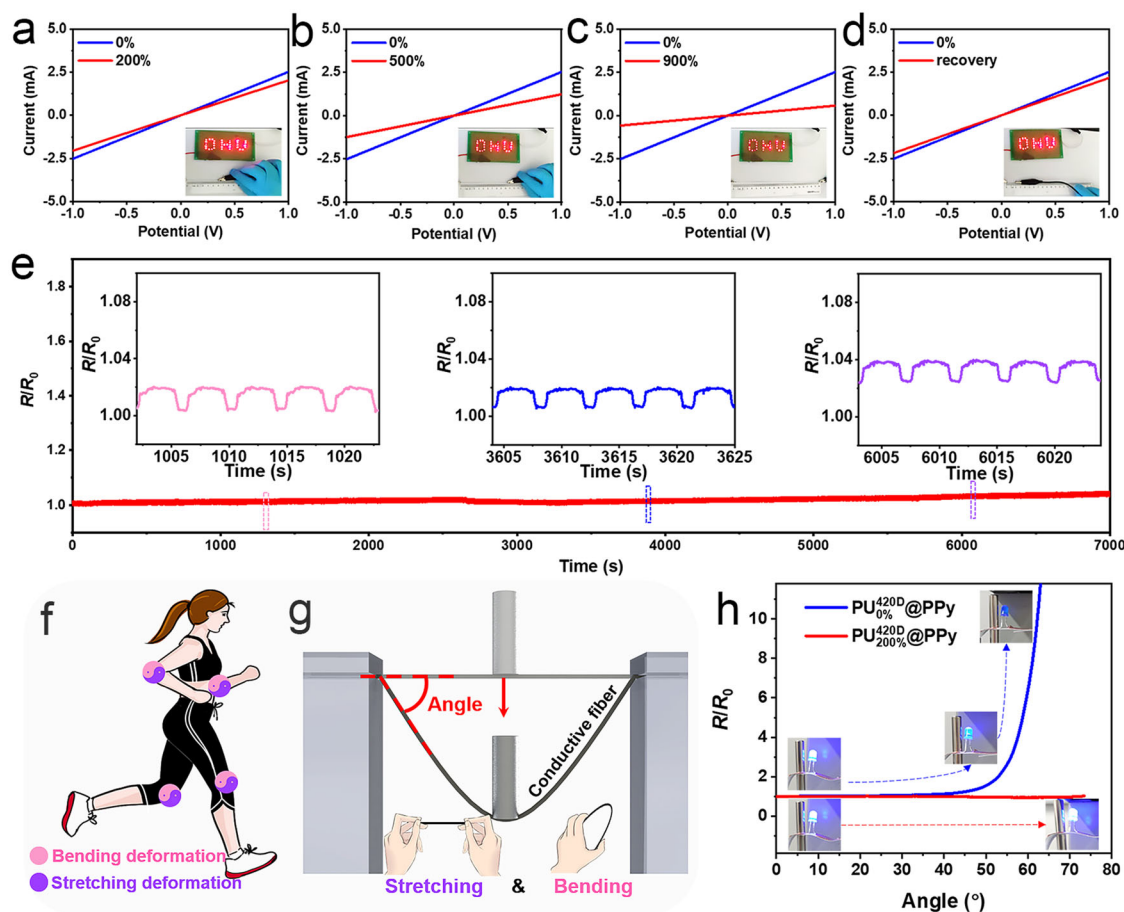
Fig. 5 Conductivity stability of the PU$_{200\%}^{420D}$@PPy. a–d The *I-V* curves of PU$_{200\%}^{420D}$@PPy at different strains (200%, 500%, 900%, and recovery). **e** The 1500 cyclic loading-unloading test of PU$_{200\%}^{420D}$@PPy under 20% strain. Inset shows 5 cycles at the beginning and the end of the 1500 cycles, respectively. **f** Schematics for dual bending (pink) and stretching (purple) deformation for human body movement. **g** Stretching-bending instrument for the filament. **h** Real-time resistance change of the filament during a stretching-bending process.

difference between theoretical and experimental results in the first stage may be due to the volume change of PPy coating under the pressure between monofilaments along the cross-section direction during the buckle expansion process.

Reversibility is a very important parameter for wearable electronic textiles. Figure 5a–d show the *I-V* curves of the PU$_{200\%}^{420D}$@PPy at different elongations. At 200% elongation, the slope of the *I-V* curve was only slightly less steep with respect to that at 0% elongation (Fig. 5a), and the LED lamp linked to the filament remained very bright (Fig. 5a inset). When the elongation reached 500%, the filament resistance increased approximately twice, and the LED began to dim (Fig. 5b). Figure 5c shows that even at 900% elongation, the filament resistance could still be used as a conductor to light up the LED lamp. This confirmed that the PU$_{200\%}^{420D}$@PPy can be reliably used as a stretchable conductor under very large strains. After recovery, the filament resistance only increased by 15% (Fig. 5d), caused by the broken PPy. Figure 5e presents the periodical change of resistance in 1500 stretch–recovery cycles with strain changed from 0% to 20%. The resistance at 0% strain only increased 3% after 1500 cycles, testifying the remarkable reversibility and stability of the PU$_{200\%}^{420D}$@PPy. To further verify the reusability of the multifilament, the conductivity of the multifilament after wash in water was characterized. The entire wash cycle of a washing machine, lasting 34 minutes, includes four steps of warm washing, rinsing, draining and drying[42]. We simulated this process using a method similar to the color fastness washing test (GB/T 3921-2008). For simplicity,

the rinsing step was replaced by a more severe warm wash step and the draining step, which did little damage to the fibers, was omitted. During a simulated washing test, therefore, the multifilament underwent a warm washing (800 rpm, 40 °C, 20 min) and a drying (60 °C, 15 min). As the number of washing increased, the conductivity gradually decreased because of the de-doping process of PPy;[43] however, the conductivity was still 94.6 S m^{-1} after 16 washes (Supplementary Fig. 18). In human body movement, stretching deformation is often accompanied by bending deformation (Fig. 5f). Therefore, resistance of the filament under both stretching and bending was also studied to better simulate human body movement. We designed a stretching-bending instrument (Fig. 5g) with an LED system to monitor the real-time change in resistance of the filament, and the results are shown in Fig. 5h. At a high bending angle of 70°, the resistance of the PU$_{200\%}^{420D}$@PPy changed only 3.5%, while the resistance of the PU$_{0\%}^{420D}$@PPy increased by 6441.6%. The PU$_{200\%}^{420D}$@PPy showed an unmatchable insensitive conductivity, as evidenced by the hardly noticeable LED brightness variations (Fig. 5f and Supplementary Video 5).

Wearable Applications
The actual conductivity is another important factor besides the quality factor that affects the application of fiber conductors to wearable circuit system. As for the application in 3D and 2D stretchable conductive materials, our small diameter conductive multifilament can be used to manufacture more compact,
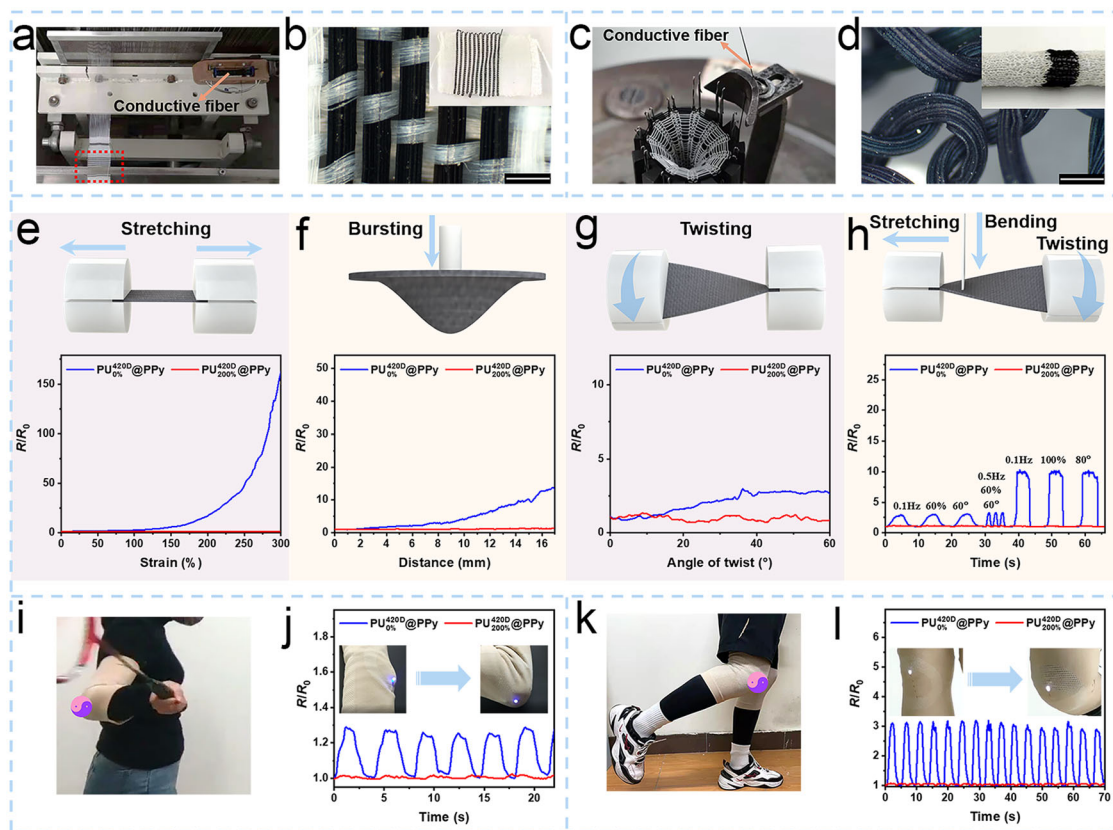
Fig. 6 Integration of PU$_{200\%}^{420D}$ @PPy multifilament using textile technology and its potential applications. Optical images of **a** rapier loom machine, **b** fabric with conductive multifilament obtained by weaving, **c** circular knitting machine and **d** fabric with conductive multifilament obtained by knitting. Scale bar is 0.5 mm. Resistance changes of the fabric during **e** stretching, **f** bursting, and **g** twisting. **h** Dynamic resistance changes of the fabric under multiple deformations. Application of the fabric as stretchy electronics during **i**, **j** arm bending and **k**, **l** walking.

sophisticated electronic textiles with textile technology. Integrating several fibers into a strand by doubling and twisting, or integrating many fibers into a fabric by weaving, knitting, and embroidery is almost an essential step in the textile forming process. This is equivalent to connecting multiple conductors in parallel, resulting in a lower overall resistance. Although paralleling resistors is an effective way to improve circuit conductivity, it inevitably results in an increase in size. Benefiting from the small diameter of conductive multifilament in this work, the strands could still meet the integration requirements of compact, sophisticated electronics after paralleled. Taking the integration of several fibers into a strand by doubling and twisting as an example, assuming that the fiber cross-section is circular and ignoring the extrusion deformation between fibers, according to the closest packing theory, the resistance of the strand obtained by twisting 7 fibers is reduced by a factor of 7, while the diameter is only increased by a factor of three. To test our hypothesis, a strand formed by twisting 7 conductive multifilaments was fabricated. The diameter of the conducting fibers was about 0.65 mm (Supplementary Fig. 19a) and the initial resistance was about one-seventh of that of PU$_{200\%}^{420D}$ @PPy (Supplementary Fig. 19b), which is consistent with the theoretical model. Importantly, the fineness of the strands is better than that of the previously reported fiber conductors, and the electrical conductivity is also comparable[8,12,41]. To further validate the potential application in wearable circuits, an LED system with the strands formed by twisting 16 conductive multifilaments as a circuit was designed. The LEDs could be visually observed to be lit at 3 V (Supplementary Fig. 19c), indicating negligible energy loss in the circuit.

Similarly, integrating many fibers into a fabric by weaving, knitting, and embroidery is an effective way to improve circuit

conductivity. To demonstrate the feasibility of preparing compact, sophisticated electronic textiles, textile fabrics manufactured with the conductive multifilament by weaving, knitting, and embroidery, respectively (Fig. 6a–d and Supplementary Fig. 20). The rapier loom and circular knitting machines used were shown in Fig. 6a & c. Different fiber paths (loops or straight lines, Fig. 6b & d) and fiber arrangements (Supplementary Fig. 20a and Fig. 6b), different fabric shapes (sheets or tubes, Fig. 6b & d inset) and complex patterns (Supplementary Fig. 20b) can be easily produced through textile technology. The plain weave fabrics with the PU$_{0\%}^{420D}$ @PPy or PU$_{200\%}^{420D}$ @PPy as the wefts were used to evaluate the functionality of the conductive multifilament after weaving (Fig. 6a & b) because weaving with textile forming technologies causes the greatest abrasion on the PPy coating. Supplementary Fig. 21 shows that the initial resistance of the fabric integrated by four PU$_{200\%}^{420D}$ @PPy is reduced to about a quarter of the resistance of a single fiber. Moreover, changes in resistance (R/R_0) during stretching, bursting and twisting were also evaluated to simulate the robust deformations when used in wearable electronic textiles. Figure 6e reveals that the R/R_0 of the fabric integrated with the PU$_{200\%}^{420D}$ @PPy was only 1.46 under 300% strain, which was much lower than that of the fabric composed of the PU$_{0\%}^{420D}$ @PPy (170.78), indicating that the fabric inherited the strain-insensitive behavior of the original conductive multifilament. The bursting process, that is, applying a vertical strain to the fabric, cannot be ignored for smart textiles. A device to apply the vertical strain was designed and the change in resistance of the fabric during the bursting process is shown in Fig. 6f. When the rod (diameter: 5 mm) perpendicular to the fabric (20 mm × 20 mm) descended to 17 mm, the resistance of the deformed fabric composed of the PU$_{200\%}^{420D}$ @PPy only increased by 30% while

the resistance of fabric composed of the $PU^{420D}_{0\%}$ @PPy increased by 1225%. Also, as shown in Fig. 6g, the electrical resistance of the fabric composed of the $PU^{420D}_{200\%}$ @PPy displayed little dependence on torsion deformation compared to the fabric composed of the $PU^{420D}_{0\%}$ @PPy. The motion of human body is complex and often results in multiple deformations of the wearables. Therefore, we designed a device that can simultaneously generate multiple deformations such as stretching, bending and twisting to simulate the complex deformations during real human body motion (Supplementary Video 6). The resistance of the fabric under test exhibited periodic changes as a function of the periodic loading and unloading of the complex deformations (Fig. 6h). Under different frequencies and deformations, the resistance of the fabric composed of the $PU^{420D}_{200\%}$ @PPy revealed little change compared to the fabric composed of the $PU^{420D}_{0\%}$ @PPy. These results illustrate that the fabric composed of the $PU^{420D}_{200\%}$ @PPy can meet the challenge of the complex movement of human body.

Furthermore, we integrated the conductive multifilament fibers into commercial elbow and knee pads through embroidery, to verify if the electrical stability is reliable under large deformations in real human motions. The real-time changes of R/R_0 of the elbow pad (Fig. 6i) equipped with the $PU^{420D}_{0\%}$ @PPy or the $PU^{420D}_{200\%}$ @PPy are shown in Fig. 6j. The change of the $PU^{420D}_{200\%}$ @PPy pad was negligible while that of the $PU^{420D}_{0\%}$ @PPy pad showed a good linearity and repeatability under the periodic bending of the elbow. There was almost no change in the brightness of the LED light in Fig. 6j inset, confirming the strain-insensitive conductivity of the elbow pads equipped with the $PU^{420D}_{200\%}$ @PPy. Compared with the elbow, the knee underwent a greater strain during exercise, resulting in obvious changes in resistance (Fig. 6k). Despite this, the knee pads equipped with the $PU^{420D}_{200\%}$ @PPy still showed an outstanding insensitive behavior; and the LED lights also showed constantly visible brightness during exercise (Fig. 6l and Supplementary Video 7). Therefore, the conductive PU multifilament with the PPy buckling structure in parallel is a strong candidate to build electronic circuits in stretchable and wearable electronic fabrics.

In summary, we designed and produced a conductive PU multifilament with the PPy buckling structure in parallel by a pre-stretching and in situ polymerization method. The pretreatment of the PU multifilament with PDA improved the wettability so that PPy could be polymerized uniformly on surface of the monofilaments. Releasing the pre-stretch after polymerization generated a parallel buckling PPy structure. Besides, the addition of NaSSA into PPy can improve the stretchability. The highly stretchable $PU^{420D}_{200\%}$ @PPy multifilament exhibited a high initial conductivity (238.0 S m^{-1}), a small diameter (0.21 mm), a high Q value (10.9) at 200% strain, and a high reversibility in electrical response in a wide range of deformation up to 900% strain ($Q = 2.6$). Moreover, the multifilament can be easily integrated into smart textiles through the existing textile technologies and maintain its high strain-insensitive behavior during the robust human body movement. This conductive multifilament therefore shows a great potential in wearable electrical devices.

METHODS
Materials
This study did not generate new unique reagents. The PU multifilaments (40D, 140D, 210D, 420D, 840D) were purchased from Jiaxing Xinhai Textile Co., Ltd. (Zhejiang, China). Pyrrole (Py, 98+%, Alfa Aesar) was purchased from Shanghai Yishi Chemical Co., Ltd. (Shanghai, China). Py was distilled twice under reduced pressure and stored at 4 °C in dark before use. Iron trichloride hexahydrate (FeCl$_3$·6H$_2$O), anhydrous ethanol, tris(hydroxy-methyl)methyl aminomethane (>99%), cyclohexane, hydrochloric acid (HCl, chemically pure) were obtained from Sinopharm Chemical Reagent Co., Ltd. (Shanghai, China). Sodium sulfosalicylate (NaSSA, Rhawn) and dopamine (DA, Sigma) were provided by Wendong (Shanghai) Chemical Co., Ltd. (Shanghai, China). All chemicals were analytical reagents and used without further purification unless otherwise stated.

Fabrication of Conductive PU Multifilament with Buckling Structure
About one meter of the PU multifilament under stretch (0%, 50%, 100%, 200%, or 300%) was immersed in a DA solution (2 mg mL^{-1}, 50 mM Tris-HCl buffer, and pH 8.5) for 5 min in ultrasonic and then reacted for 8 h. After washing, it was placed in a dish (diameter: 90 mm) containing of a FeCl$_3$·6H$_2$O (0.36 M) and NaSSA (0.36 M) water solution (20 mL), and then frozen at −20 °C. After, cyclohexane (19.5 mL) containing of Py (0.5 mL) was transferred onto the top of the above solution. The polymerization in situ was maintained for different times (6 h, 12 h, 18 h, 24 h, or 36 h) at 2 °C. At the end of polymerization, the PU@PPy multifilament was washed several times with anhydrous ethanol and then with deionized water, followed by ultrasonic washing in water for 5 min. Finally, the strain of the PU multifilament was released to form the PU@PPy with a buckling structure. The filament was dried at room temperature.

Fabrication of Conductive Fabric
Woven fabrics with PET filaments as warp, PU and PU^{420D}_y @PPy as weft were fabricated by a rapier loom (ASL2300, Suzhou Shuohai Electro-mechanical Technology Co., Ltd., Suzhou, China). Knitted fabrics made of PU and PU^{420D}_y @PPy filaments were fabricated by a circular knitting machine (Biomedical Textiles Lab, Donghua University, Shanghai, China). Embroidery fabric is realized by hand sewing the PU^{420D}_y @PPy filament onto a knitted fabric.

Characterizations
The morphology of the samples was observed by scanning electron microscopy (SEM, Hitachi SU8010, Tokyo, Japan) at an accelerating voltage of 5 kV. Before observation, the specimens were sputter-coated with gold (Hitachi Ion Sputter MC1000, Tokyo, Japan). The cross-section of the multifilament was obtained by breaking it in liquid nitrogen. An atomic force microscope (AFM, 5500AFM-SPM, Agilent, California, USA) was further used to analyze the multifilaments by immobilizing the specimen on a glass slide with double-sided tape. In situ tensile testing was performed using the Phenom XL equipped with a tensile holder (Phenom XL, Phenom-Scientific, Shanghai, China).

The macroscopic appearance of the fabric was obtained by a stereoscopic microscope (Nikon SMZ745T, Tokyo, Japan). A Fourier transform near-infrared spectrometer (FT-NIR, Antaris II, Thermofisher, Waltham, USA) in attenuated total reflection (ATR) mode was used to characterize the chemical composition of the samples. The surface chemical composition of samples was investigated by an X-ray photo-electron spectrometer (XPS, Escalab250xi, Thermofisher, Waltham, USA) with Al Kα radiation ($\lambda = 8.34$ Å) as the excitation source. Raman spectra were collected with a Raman micro spectrometer (inVia-Reflex, Renishaw, Gloucestershire, UK) equipped with a He-Ne$^+$ laser emitting at 633 nm.

The mechanical properties of the PPy films with a width of 5 mm were tested using a Single Fiber Strength Tester (YG-001, Wenzhou Fangyuan Instrument Co., Ltd., Wenzhou, China) at 10 mm gauge length and 10 mm min^{-1} crosshead speed. According to the cantilever beam theory, 20 mm of a 30 mm long PPy film was extended out of the edge of a table to form a cantilever beam. The angle formed between the suspended film and the table surface was measured to evaluate the flexibility of the PPy films. The tensile properties of the multifilament were investigated using a single fiber strength tester (LLY-06E, Laizhou Electron Instrument Co., Ltd., Laizhou, China) at 5 mm gauge length and a strain rate of 50 mm min^{-1}. Rough silicone sheets were fixed at both ends of the filaments to prevent sliding during the test. The cyclic stretching of the PU^{420D}_y @PPy multifilament was tested by a Spandex elastic tester (XN-1A, Shanghai New Fiber Instrument Co., Ltd., Shanghai, China) at a distance of 50 mm and a speed of 100 mm min^{-1}. The diameter of the filaments was measured with a latex thickness meter (CH-12.7-BTSX, Shanghai Liuling Instrument Factory, Shanghai, China). All tests were performed under standard environmental conditions (20 ± 1 °C, RH 65% ± 2%), and at least three specimens were tested for each sample.

For thermostability test, approximately 3 mg of samples was heated from 50 to 800 °C at a heating rate of 20 °C min^{-1} under a nitrogen atmosphere using a thermogravimetric analyzer (TGA8000, Thermofisher, Waltham, USA).

To characterize the washability of the PU_y^{420D}@PPy multifilament, samples of 15 cm in length were stirred in water (40 °C) with a speed of 800 r min^{-1} for 20 min and then dried at 60 °C.

To monitor the change in resistance during deformation, the two ends of the conductive filament or the conductive fabric were connected to a conductive copper tape with the help of a rough silicone sheet. Then the conductive copper tape was connected to a source meter unit (Keithley 2450, Tektronix, Cleveland, USA) to monitor the change of the resistance during the deformation. This work is not about living individuals and does not include collection of individually identifiable private information, therefore, the Institutional Review Board approval was not a prerequisite. And we have obtained informed consent from all participants.

DATA AVAILABILITY

The data that support the findings of this study are available from the corresponding author upon reasonable request.

REFERENCES

1. Zhao, X.-F. et al. Spider web-like flexible tactile sensor for pressure-strain simultaneous detection. ACS Appl. Mater. Interfaces 13, 10428–10436 (2021).
2. Liu, Z. et al. Highly breathable and stretchable strain sensors with insensitive response to pressure and bending. Adv. Funct. Mater. 31, 2007622 (2021).
3. Kim, T. et al. Supersonically sprayed washable, wearable, stretchable, hydrophobic, and antibacterial rgo/agnw fabric for multifunctional sensors and supercapacitors. ACS Appl. Mater. Interfaces 13, 10013–10025 (2021).
4. Chai, Z. et al. Tailorable and wearable textile devices for solar energy harvesting and simultaneous storage. Acs Nano 10, 9201–9207 (2016).
5. Jo, A. et al. Textile resistance switching memory for fabric electronics. Adv. Funct. Mater. 27, 1605593 (2017).
6. Shi, X. et al. Large-area display textiles integrated with functional systems. Nature 591, 240–245 (2021).
7. Zhang, M. et al. Weft-knitted fabric for a highly stretchable and low-voltage wearable heater. Adv. Electron. Mater. 3, 1700193 (2017).
8. Sun, F. et al. Stretchable conductive fibers of ultrahigh tensile strain and stable conductance enabled by a worm-shaped graphene microlayer. Nano Lett. 19, 6592–6599 (2019).
9. Uzun, S. et al. Knittable and washable multifunctional mxene-coated cellulose yarns. Adv. Funct. Mater. 29, 1905015 (2019).
10. Gao, Y. et al. Winding-locked carbon nanotubes/polymer nanofibers helical yarn for ultrastretchable conductor and strain sensor. Acs Nano 14, 3442–3450 (2020).
11. Cheng, Y. et al. A biomimetic conductive tendril for ultrastretchable and integratable electronics, muscles, and sensors. Acs Nano 12, 3898–3907 (2018).
12. Cheng, Y., Wang, R., Sun, J. & Gao, L. Highly conductive and ultrastretchable electric circuits from covered yarns and silver nanowires. Acs Nano 9, 3887–3895 (2015).
13. Wu, X., Han, Y., Zhang, X. & Lu, C. Spirally structured conductive composites for highly stretchable, robust conductors and sensors. ACS Appl. Mater. Interfaces 9, 23007–23016 (2017).
14. Liu, Z. F. et al. Hierarchically buckled sheath-core fibers for superelastic electronics, sensors, and muscles. Science 349, 400–404 (2015).
15. Xia, S., Song, S., Jia, F. & Gao, G. A flexible, adhesive and self-healable hydrogel-based wearable strain sensor for human motion and physiological signal monitoring. J. Mat. Chem. B 7, 4638–4648 (2019).
16. Lee, D. W., Lee, J. H. & Jin, J.-H. Innovative evolution of buckling structures for flexible electronics. Compos. Struct. 204, 487–499 (2018).
17. Chen, Z. H., Fang, R., Li, W. & Guan, J. Stretchable transparent conductors: From micro/macromechanics to applications. Adv. Mater. 31, 1900756 (2019).
18. Li, L. et al. Ultrastretchable fiber sensor with high sensitivity in whole workable range for wearable electronics and implantable medicine. Adv. Sci. 5, 1800558 (2018).
19. He, C., Sun, S. & Wu, P. Intrinsically stretchable sheath-core ionic sensory fibers with well-regulated conformal and reprogrammable buckling. Mater. Horiz. 8, 2088–2096 (2021).
20. Ho, M. D., Liu, Y., Dong, D., Zhao, Y. & Cheng, W. Fractal gold nanoframework for highly stretchable transparent strain-insensitive conductors. Nano Lett. 18, 3593–3599 (2018).
21. Lee, J. et al. Intrinsically strain-insensitive, hyperelastic temperature-sensing fiber with compressed micro-wrinkles for integrated textronics. Adv. Mater. Technol. 5, 2000073 (2020).
22. Islam, G. M. N., Ali, A. & Collie, S. Textile sensors for wearable applications: A comprehensive review. Cellulose 27, 6103–6131 (2020).
23. Liu, Y. et al. Capillary-force-induced cold welding in silver-nanowire-based flexible transparent electrodes. Nano Lett. 17, 1090–1096 (2017).
24. Bi, S., Hou, L. & Lu, Y. Multifunctional sodium alginate fabric based on reduced graphene oxide and polypyrrole for wearable closed-loop point-of-care application. Chem. Eng. J. 406, 126778 (2021).
25. Lv, J. et al. High-performance textile electrodes for wearable electronics obtained by an improved in situ polymerization method. Chem. Eng. J. 361, 897–907 (2019).
26. Mao, J., Li, C., Park, H. J., Rouabhia, M. & Zhang, Z. Conductive polymer waving in liquid nitrogen. Acs Nano 11, 10409–10416 (2017).
27. Zhang, Q. et al. Ultra-low temperature flexible supercapacitor based on hierarchically structured pristine polypyrrole membranes. Chem. Eng. J. 420, 129712 (2021).
28. Wang, Y. et al. A highly stretchable, transparent, and conductive polymer. Sci. Adv. 3, e1602076 (2017).
29. Dauginet-Da Pra, L. & Demoustier-Champagne, S. Investigation of the electronic structure and spectroelectrochemical properties of conductive polymer nanotube arrays. Polymer 46, 1583–1594 (2005).
30. He, H. et al. Biocompatible conductive polymers with high conductivity and high stretchability. ACS Appl. Mater. Interfaces 11, 26185–26193 (2019).
31. Popescu, S., Ungureanu, C., Albu, A. M. & Pirvu, C. Poly(dopamine) assisted deposition of adherent ppy film on ti substrate. Prog. Org. Coat. 77, 1890–1900 (2014).
32. Song, C. et al. An injectable conductive three-dimensional elastic network by tangled surgical-suture spring for heart repair. Acs Nano 13, 14122–14137 (2019).
33. Yang, T., Zhou, W. & Ma, P. Manufacture and property of warp-knitted fabrics with polylactic acid multifilament. Polymers 11, 65 (2019).
34. Zheng, L. et al. Conductance-stable liquid metal sheath-core microfibers for stretchy smart fabrics and self-powered sensing. Sci. Adv. 7, eabg4041 (2021).
35. Zhu, S. et al. Ultrastretchable fibers with metallic conductivity using a liquid metal alloy core. Adv. Funct. Mater. 23, 2308–2314 (2013).
36. Kim, A., Ahn, J., Hwang, H., Lee, E. & Moon, J. A pre-strain strategy for developing a highly stretchable and foldable one-dimensional conductive cord based on a ag nanowire network. Nanoscale 9, 5773–5778 (2017).
37. Zhao, Y. et al. A moss-inspired electroless gold-coating strategy toward stretchable fiber conductors by dry spinning. Adv. Electron. Mater. 5, 1800462 (2019).
38. Qu, Y. et al. Superelastic multimaterial electronic and photonic fibers and devices via thermal drawing. Adv. Mater. 30, 1707251 (2018).
39. Zhang, B. et al. Stretchable conductive fibers based on a cracking control strategy for wearable electronics. Adv. Funct. Mater. 28, 1801683 (2018).
40. Lee, S. et al. Ag nanowire reinforced highly stretchable conductive fibers for wearable electronics. Adv. Funct. Mater. 25, 3114–3121 (2015).
41. Zhang, Z. et al. Superelastic supercapacitors with high performances during stretching. Adv. Mater. 27, 356–362 (2015).
42. Wicaksono, I. et al. A tailored, electronic textile conformable suit for large-scale spatiotemporal physiological sensing in vivo. npj Flex. Electron. 4, 5 (2020).
43. Fonner, J. M. et al. Biocompatibility implications of polypyrrole synthesis techniques. Biomed. Mater. 3, 034124 (2008).

AUTHOR CONTRIBUTIONS

L.Y., and M.J. conceived the project; L.Y., G.Y., Wei L., and S.M. carried out the preparation and measurement of stretchable fibers; L.Y., L.L., Z.Q., G.L., and W.F. assisted the result analysis; M.J. and Wang L. supervised the project; L.Y. wrote the paper with support from M.J. and Z.Z.. All authors contributed to the general discussion.

COMPETING INTERESTS
The authors declare no competing interests.

ADDITIONAL INFORMATION
Supplementary information The online version contains supplementary material available at https://doi.org/10.1038/s41528-022-00176-6.

Correspondence and requests for materials should be addressed to Jifu Mao.

Reprints and permission information is available at http://www.nature.com/reprints

Publisher's note Springer Nature remains neutral with regard to jurisdictional claims in published maps and institutional affiliations.